Accepted Manuscript

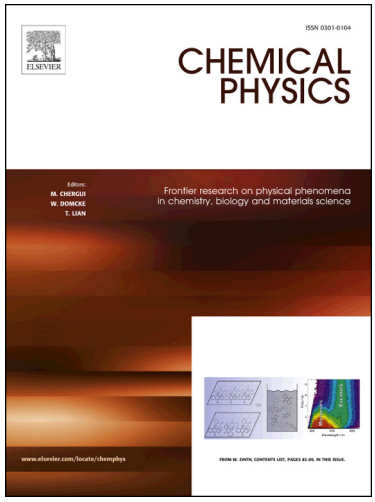

Electronic structures and population dynamics of excited states of xanthione and its derivatives

Roman G. Fedunov, Marina V. Rogozina, Svetlana S Khokhlova, Anatoly I. Ivanov, Sergei A. Tikhomirov, Stanislav L. Bondarev, Tamara F. Raichenok, Oleg V. Buganov, Vyacheslav K. Olkhovik, Dmitrii A. Vasilevskii

PII: S0301-0104(17)30337-3
DOI: http://dx.doi.org/10.1016/j.chemphys.2017.07.007
Reference: CHEMPH 9827

To appear in: *Chemical Physics*

Please cite this article as: R.G. Fedunov, M.V. Rogozina, S.S. Khokhlova, A.I. Ivanov, S.A. Tikhomirov, S.L. Bondarev, T.F. Raichenok, O.V. Buganov, V.K. Olkhovik, D.A. Vasilevskii, Electronic structures and population dynamics of excited states of xanthione and its derivatives, *Chemical Physics* (2017), doi: http://dx.doi.org/10.1016/j.chemphys.2017.07.007

This is a PDF file of an unedited manuscript that has been accepted for publication. As a service to our customers we are providing this early version of the manuscript. The manuscript will undergo copyediting, typesetting, and review of the resulting proof before it is published in its final form. Please note that during the production process errors may be discovered which could affect the content, and all legal disclaimers that apply to the journal pertain.

ACCEPTED MANUSCRIPT

Electronic structures and population dynamics of excited states of xanthione and its derivatives

Roman G. Fedunov[a], Marina V. Rogozina[a], Svetlana S Khokhlova[a], Anatoly I. Ivanov[a,*], Sergei A. Tikhomirov[b], Stanislav L. Bondarev[b], Tamara F. Raichenok[b], Oleg V. Buganov[b], Vyacheslav K. Olkhovik[c], Dmitrii A. Vasilevskii[c]

[a] *Volgograd State University, University Avenue 100, Volgograd 400062, Russia*
[b] *B.I. Stepanov Institute of Physics, National Academy of Sciences of Belarus, 68 Prospekt Nezavisimosti, Minsk BY-220072, Republic of Belarus*
[c] *Institute of Chemistry of New Materials, National Academy of Sciences of Belarus, 36, Fr. Skaryna Street, Minsk BY-220141, Republic of Belarus*

Abstract

A new compound, 1,3-dimethoxy xanthione (DXT), has been synthesized and its absorption (stationary and transient) and luminescence spectra have been measured in n-hexane and compared with xanthione (XT) spectra. The pronounced broadening of xanthione vibronic absorption band related to the electronic transition to the second singlet excited state has been observed. Distinctions between the spectra of xanthione and its methoxy derivatives are discussed. Quantum chemical calculations of these compounds in the ground and excited electronic states have been accomplished to clarify the nature of electronic spectra changes due to modification of xanthione by methoxy groups. Appearance of a new absorption band of DXT caused by symmetry changes has been discussed. Calculations of the second excited state structure of xanthione and its methoxy derivatives confirm noticeable charge transfer (about 0.1 of the charge of an electron) from the methoxy group to thiocarbonyl group. Fitting of the transient spectra of XT and DXT has been fulfilled and the time constants of internal conversion $S_2 \rightarrow S_1$ and intersystem crossing $S_1 \rightarrow T_1$ have been determined. A considerable difference between the time constants of internal conversion $S_2 \rightarrow S_1$ in XT and DXT is uncovered.

Keywords: higher excited states, molecular electronic devices, charge transfer

*Corresponding author. Tel. +7-8442-464894. E-mail: Anatoly.Ivanov@volsu.ru

ACCEPTED MANUSCRIPT

ACCEPTED MANUSCRIPT

1. INTRODUCTION

Development of molecular scale electronic devices is one of the most promising contemporary technologies in microelectronics [1, 2]. The organic molecules can be used to construct such key electronic devices as spatial light modulators, thin-film transistors, light-emitting diodes, sensors, solar cells, optical switches and others [3]. Among these molecular size electronic devices the optical switches are one of the most challenging. The nanoscale electronic switches can open the new generation of tiny electronic devises far beyond the modern silicon-based technology [4].

The optical switches are the particular devices capable to switch between two stable and selectively chosen states with different physical properties which can be flipped by the direct optical impulse. Molecular triad of type acceptor$_L$–donor–acceptor$_R$ ($A_L - D - A_R$) is one of the possible implementations of optical switches [5]. In such molecular triads there are two locally excited electronic states of donor enabling the electron transfer to selectively switch between "right" (A_R) or "left" (A_L) acceptor addressing to the wavelength of excitation pulse. The molecular systems in which the photoreactions involving some excited states may proceed are intensively investigated during past decade [6, 7, 8, 9, 10, 11, 12, 13, 5, 14, 15, 16, 17, 18, 19, 20]. The latest researches [5, 14, 15] were focused on molecular switches based on systems where zinc-porphyrin (ZnP) and imide play the role of electron donor and electron acceptor, respectively. The principal challenge being interfered the development of optical switches containing ZnP-imide systems is a problem of low ions quantum yield of photoinduced charge transfer (PCT) from the second excited state S_2 of ZnP to the covalently-bounded acceptor. The results of computer simulations of PCT in such systems [14, 15, 18] show that the low efficiency of charge separation is determined by the ultrafast recombination to the first excited state of ZnP during the "hot" stage when nuclear subsystems of reactants and solvent are far from equilibrium. All known studies of PCT demonstrate low quantum yield of thermalized ion products (about 20%) from the second excited state despite the fact that the rate of electron transfer significantly exceeds the rate of non-radiative relaxation [5]. Thus, the yield of ionic products is limited by the ultrafast ion recombination to the first excited state S_1. The conclusion is confirmed by the experimental data showing that ultrafast fluorescence decay of second excited state being accompanied by the competing fluorescence decay from the first excited state.

ACCEPTED MANUSCRIPT

Since the lifetime of the second excited state of the ZnP derivatives is not strongly shorter than the characteristic time of internal conversion (approximately 2 ps) the quantum yield of charge separation states is considerably less than unity. The strong coupling between the local excited S_2 and ionic states is necessary for effective competition between charge transfer and internal conversion. That causes in the effectiveness of hot charge recombination to the S_1 state [14, 15]. The latest results attest that the high quantum yield of thermalized ionic state can be only achieved in molecular systems with lifetimes of S_2 state significantly greater than 2 ps.

Molecular systems based on azulene or thioketone derivatives may be used as an alternative to the systems containing ZnP-imide. According to Refs. [8] research of mechanisms of luminescence quenching in azulene faces even greater complexity. Despite the longer lifetime of S_2 state (approximately few nanoseconds) the definition of the states where the electron passes to is complicated due to the interference of ion absorption spectra with absorption of azulene from S_2 [21]. The measurement of the kinetics of S_1 population is also problematic in consequence of its short lifetime (less than 1 ps). It was ascertained that the internal conversion to the ground state is the primary channel of the S_1-state decay. Hence at the moment the thioketones looks more promising as a compounds of the optical molecular switches. Their S_2 lifetimes can be as large as hundred picoseconds [21] therefore the S_2-state quenching, that is, photoinduced charge separation, can be much more effective than that in porphyrins. For example, the lifetime of S_1-state of xanthione (XT) molecule is short but it decays into the triplet state with quantum yield close to 1. In literature there is some information on the electron structure and optical spectra of XT [22, 23, 24] whereas donor-acceptor dyads and triads containing XT are still not studied. A rather effective bimolecular electron transfer quenching of xanthione S_2 state by series of electron donor in acetonitrile solution was observed [8].

Thus, to develop effective high-speed optical molecular switches the next steps would be essential: 1) theoretical study of molecular structures to select potentially perspective heterocyclic compounds with electron-donor or electron-acceptor substituents; 2) synthesis and following experimental and theoretical research of physical and chemical properties of the compounds suitable for constructing molecular electronic devices.

The aims of this paper are: (i) measurements and analysis of stationary absorption and luminescence spectra of XT and its newly synthesized methoxy derivatives, (ii) quantum chemical calculations of energetic struc-

ACCEPTED MANUSCRIPT

ture and geometry of XT and a few of its methoxy derivatives, (iii) measurements and analysis of transient spectra of XT and 1,3-dimethoxy xanthione (DXT), (iv) fitting of the transient spectra of XT and DXT and calculation of the second excited state lifetime, (v) determination of the time constants of internal conversion $S_2 \rightarrow S_1$ and intersystem crossing $S_1 \rightarrow T_1$.

2. METHODOLOGY

2.1. Computational methods

The simulations were performed using MOPAC 2016 [25, 26, 27, 28]. A semiempirical Parametric Method Number 3 (PM3) [25, 29] was used to provide full geometry optimization and compute electronic structures of XT molecule and its methoxy derivatives. The choice of PM3 is justified by the fact that the method was parameterized for enthalpy and geometry characteristics calculations of the molecules similar to benzene [27]. The systems considered here belong to the same class. The calculations of the heat of formation ($\Delta_f H^\circ$) were carried out in the approximation of isolated molecule in the gas phase at 298 K. COSMO [30] solvent model was employed to take it implicitly into the account. Hexane with dielectric permittivity EPS = 1.89 was chosen as a solvent.

Approach based on the many-electron configuration interaction MECI [31] was used to calculate the vertical energies of transitions to the ground electronic state. To specify the number of occupied energy levels in MECI calculation the MOPAC keyword value for configuration interaction calculations, C.I., is chosen to be: 4, 6, 8 and 9. The approach allows the excited states energy calculation accounting for solvent within the COSMO solvent model. Additionally it takes into account the quadratic influence of the refractive index on the dielectric energy of the excited states. In the calculations we used following value of keyword accounting for squared refractive index: $\mathrm{N} * * 2 = 1.89$. The rest of the parameters was chosen to be default.

2.2. Experimental methods

Xanthion was synthesized from xanthone being acted by the Lawessons reagent. The xanthone dimethoxy derivative (1,3-dihydroxy-xanthone) was synthesized in the reaction of phloroglucinol with salic acid in presence of fresh melted zinc chloride and phosphate chloride. Obtained 1,3-dihydroxy xanthone acting with excess of dimethyl sulfate in presence of potassium carbonate produces 1,3-dimethoxy xanthone. The latter smoothly turns into

ACCEPTED MANUSCRIPT

DXT being acted by the Lawassons reagent. Registration of the electronic absorption and luminescence spectra of compounds was carried out in 1 cm quartz cuvettes by spectrophotometer Cary-500 (USA) and spectrofluorimeter (Solar, Belarus). n-hexane (Aldrich, USA) was used as a solvent.

In the literature there is large scattering of the values of molar extinction coefficient [32]. This is the reason why this quantity was measured in this work. Molar extinction coefficients were determined by weighing three samples for each thioketone and subsequent dissolving in certain volume of n-hexane. The electronic spectra were recorded for obtained solution of XT and DXT using spectrometer Cary-500 (USA). The oscillator strengths shown in Table 3 of the manuscript were calculated using the following equation [33]:

$$f = 1.3 \cdot 10^{-8} \frac{9n}{(n^2+2)^2} \int \varepsilon(\nu) d\nu$$

where n is the refractive index of the solvent (for n-hexane $n = 1.375$), $\varepsilon(\nu)$ is the molar extinction coefficient, and ν is the wave number in cm^{-1}.

Pump-probe measurement setup was exploited as described elsewhere [34, 35]. The laser pulses of 140 fs duration of the second harmonic of $Al_2O_3 : Ti^{3+}$ laser (395 nm) with the energy in a range 10 – 30 μJ was used us a pump. A 2 mm thick cell filled with a solvent at a dye concentration of 10^{-4} M was utilized as a sample. The probe was a white continuum ranging from 400 nm to 1100 nm generated in water by a fraction of the fundamental laser beam at 790 nm. The spectra of the signal probe and reference pulses were recorded by a polychromator equipped with silicon CCD matrix and transmitted to a computer. The differential absorbance signal $\Delta D(\lambda, \Delta t)$ is obtained as $\Delta D(\lambda, \Delta t) = \lg(\widetilde{T}_0/\widetilde{T})$, where $\widetilde{T} = E_{prob}/E_{ref}$ and $\widetilde{T}_0 = E^0_{prob}/E^0_{ref}$ are the energy ratios of the probe and reference pulses passed through the sample with and without preceding pump, respectively. The pump and the probe beam diameters of 1 mm and 0.7 mm, respectively, with nearly Gauss intensity distribution have been controlled by a CCD camera. To show the stability of samples the stationary absorption spectra were measured before and after pump-probe measurements. No changes were detected. The transient spectra were corrected for the group velocity dispersion of the probe pulse. The group velocity dispersion function has been measured, a software was elaborated to automatically account for this correction.

For stationary measurements the concentrations of molecular oxygen, XT and DXT dissolved in n-hexane are $C_{O2} = 1.56 \cdot 10^{-2}$ mol/L, $C_{XT} =$

ACCEPTED MANUSCRIPT

$C_{DXT} = 2 \cdot 10^{-5}$ mol/L, correspondingly. For non-stationary measurements the concentrations of XT and DXT are $C_{XT} = C_{DXT} = 10^{-4}$ mol/L. The excitation wavelength is $\lambda_{exc} = 340$ nm.

3. RESULTS AND DISCUSSION

3.1. Energetic and electronic properties of xanthione derivatives

Table 1: Physical characteristics of methoxy derivatives of XT in the ground state. Here $\Delta_f H^\circ$ (in kcal/mol), E_{tot}, IP, E_{HOMO}, E_{LUMO} (in eV), μ (in Db) are the formation heat, total energy, ionization potential, energy of the highest occupied molecular orbital, energy of the lowest unoccupied molecular orbital, dipole moment, respectively.

No	Comp.	R_1	R_2	A_1	A_2	$\Delta_f H^\circ$ ($\Delta_f H^\circ_{gas}$)	E_{tot}	μ	IP	E_{HOMO}	E_{LUMO}
1	I	H	H	119.8	119.7	52.60 (54.19)	-2140.964	4.11	9.00	-9.009	-1.973
2	II	H_3CO(cis)	H	114.0	119.7	13.16(15.22)	-2583.905	3.66	8.95	-8.955	-1.914
3	II	H_3CO(trans)	H	117.9	119.7	13.05(15.12)	-2583.910	5.54	8.94	-8.943	-1.908
4	III	H_3CO(cis)	H_3CO	113.9	122.8	-17.20(-14.52)	-3026.452	4.45	8.80	-8.805	-1.714
5	III	H_3CO(trans)	H_3CO	125.1	122.9	-17.46(-14.85)	-3026.464	5.05	8.80	-8.806	-1.713
6	IV	H_3CO(cis)	H_3CO(cis)	125.1	113.6	-24.78(-22.43)	-3026.781	2.87	8.92	-8.927	-1.946
7	IV	H_3CO(cis)	H_3CO(trans)	125.2	125.1	-23.97(-21.47)	-3026.746	4.34	8.91	-8.919	-1.922
8	IV	H_3CO(trans)	H_3CO(cis)	125.3	113.7	-24.92(-22.56)	-3026.781	2.87	8.92	-8.927	-1.946
9	IV	H_3CO(trans)	H_3CO(trans)	125.2	125.1	-24.09(-21.57)	-3026.751	6.47	8.90	-8.906	-1.916

Table 2: The atomic charges of the XT skeleton. The charges are presented in the units of the elementary charge. The numbers in the first column correspond to the numeration of conformers given in Table 1.

No	C_1	C_2	C_3	C_4	C_5	C_6	C_7	C_8	C_9	C_{10}	C_{11}	C_{12}	C_{13}	O	S
1	-0.1	-0.04	-0.03	0.07	-0.11	-0.05	0.11	0.07	-0.03	-0.04	-0.10	-0.05	-0.11	-0.08	-0.42
2	-0.14	-0.03	-0.10	0.10	-0.19	0.14	0.10	0.06	-0.01	-0.002	-0.10	-0.04	-0.11	-0.07	-0.40
3	-0.14	-0.06	-0.07	0.11	-0.17	0.10	0.10	0.10	-0.02	-0.02	-0.09	-0.04	-0.12	-0.07	-0.41
4	-0.22	0.17	-0.09	0.10	-0.22	0.15	0.10	0.04	-0.02	-0.03	-0.10	-0.06	-0.10	-0.08	-0.33
5	-0.18	0.15	-0.08	0.10	-0.25	0.15	0.10	0.04	-0.02	-0.03	-0.10	-0.06	-0.10	-0.09	-0.32
6	-0.17	-0.06	-0.07	0.11	-0.13	0.10	0.10	0.07	-0.01	-0.09	0.08	-0.05	-0.09	-0.07	-0.41
7	-0.17	-0.06	-0.08	0.11	-0.13	0.10	0.10	0.07	-0.01	-0.05	0.08	-0.09	-0.09	-0.07	-0.41
8	-0.14	-0.06	-0.06	0.11	-0.16	0.09	0.10	0.07	-0.01	-0.10	0.08	-0.05	-0.09	-0.07	-0.40
9	-0.14	-0.06	-0.06	0.11	-0.16	0.09	0.10	0.07	-0.01	-0.06	0.08	-0.09	-0.08	-0.07	-0.40

The results of energetic and electronic properties calculations of following molecules: (I) 9H-xanthene-9-thione, (II) 3-methoxy-9H-9-thione, (III) 1,3-dimethoxy-9H-xanthene-9-thione, (IV) 2,6-dimethoxy-9H-xanthene-9-thione and their possible conformers are listed in Table 1 and 2. Geometry structures of the molecules I, II and IV are shown in Fig. 1. The geometry

ACCEPTED MANUSCRIPT

characteristics of plain XT skeleton are almost stay the same with attachment of methoxy groups in cis- or trans-configurations. In Fig. 1 the parameters are shown only for compound I ($R_1 = R_2 = H$). For compounds II ($R_1 = H,\ R_2 = OCH_3$) and IV ($R_1 = OCH_3$, $R_2 = OCH_3$) the bond lengths and angles differ from that listed in Fig. 1 for values ± 0.02 Å and $\pm 2°$, respectively. Figure 2 demonstrates the geometry structure of compound III ($R_1 = OCH_3$, $R_2 = OCH_3$) characterized by considerable deformation of the XT skeleton. There is a noticeable deviation from plain structure. The latter leads a bond angle $C_2 - C_7 - C_{10}$ to vary from value 172° in the compounds I, II and IV up to 155° in the compound III. It should be also noted a significant deviation of sulfur atom from the XT skeleton plane that leads to variation of the bond angle $O - C_7 - S$ from 180° in the compounds I, II, IV to 159° in compound III. Such a deformation of the XT plane may result in appearance of the enantiomer properties for compound III.

Conformers of xanthione methoxy derivatives are defined by different arrangement of the methyl fragments of methoxy groups relatively the XT skeleton. Configuration of $C_1 - C_6 - O - CH_3$ may be in cis- or trans-positions. The angles A_1 and A_2 are shown in Figures 1 and 2 since they vary more than 2° for cis- and trans-configurations. Their values are listed in Table 1.

Values of formation heat, $\Delta_f H°$, calculated for the compounds I–IV are in good agreement with experimental values in liquid, $\Delta_f H°_{\text{liq}}$, at standard conditions for benzene and its methoxy derivatives. According to NIST database[36], the quantity of $\Delta_f H°_{\text{liq}}$ for benzene is positive and equals 49 kJ/mol[37]. Attachment of a methoxy group to benzene results in considerable decreasing the quantity $\Delta_f H°_{\text{liq}}$ and for anisole it equals -120 kJ/mol[38]. Attachment of the second methoxy group to anisole further reduces the value of $\Delta_f H°_{\text{liq}}$ and according to NIST for molecule 1,2-dimethoxy-benzene it achieves -290 kJ/mol [39]. The values of formation heat of xanthione methoxy derivatives shown in Table 1 manifest similar decreasing tendency with growing the number of attached methoxy groups. The formation heat in gas phase, $\Delta_f H°_{\text{gas}}$, at the standard conditions evaluated by NIST for the thioxanthone molecule which geometry structure close to compounds under consideration is positive and equals 95 kJ/mol [40].

Additional calculation of the thioxanthone molecule with full geometry optimization in gas phase gives the value of the heat of formation 115.5 kJ/mol which is pretty close to the experimental data. Thus we deduce that selected method reproduces the values of the heat of formation for xanthione-

ACCEPTED MANUSCRIPT

like molecules with precision ±20 kJ/mol. The heats of formations in gas and liquid phase for compounds I–IV are also shown in Table 1. The differences of $\Delta_f H^\circ$ between the gas and liquid phases for considered compounds are about $2-3$ kcal/mol. It seems that in COSMO model the hexane solvent influences negligibly on the geometry structure of the compounds.

The correlation of the ionization potential, IP, the energy of the highest occupied molecular orbital (HOMO), E_{HOMO}, and the energy of the lowest unoccupied molecular orbital (LUMO), E_{LUMO}, with NIST data is also pronounced. The ionization potentials of methoxy derivatives measured in gas phase decrease with attaching a methoxy group to the benzene: from 9.24 eV (benzene) to 8.20 eV (anisole). However the attachment of the next methoxy group to anisole influences negligibly on IP: 8.20 eV (anisole) $\rightarrow$ 8.14 eV (1,3-dimethoxy-benzene) whereas attachment of a group in the neighbor position leads to the significant decrease of IP: 7.8 eV (1,2-dimethoxy-benzene). The very similar picture one obtains with IP of the XT methoxy derivatives (Table 1).

Analysis of the Mulliken charges at atoms of XT skeleton (Table 2) shows a strong polarization of the compounds that is confirmed by high magnitudes of the dipole moments presented in Table 1. The high magnitudes of the dipole moments are also observed for all the conformers. According to the Table 2, the negative charges at the carbon atoms C_6 and C_{11} in the compound I increase by 0.2 units and become positive after attaching methoxy groups. At the same time at the oxygen atoms of the methoxy groups negative charge reaches -0.19. The latter leads to change both in magnitude and in direction of the dipole moment (see Figures 1 and 2). The influence of the methoxy group attachment on charges of the other atoms of the compounds II and IV is negligible. However in the compound III the methoxy groups attachment to the carbons C_2, C_6 affects the charges of all carbon atoms of the benzene fragment (from C_1 to C_6). The fragment is strongly polarized resulting in its distortion in comparison with the opposite benzene fragment (C_8-C_{13}). A comparison of the results of both the formation heat and the dipole moment of the compounds II and IV shows the conformers with smaller dipole moment to be energetically favorable whereas compound III to demonstrate the opposite situation.

ACCEPTED MANUSCRIPT

3.2. Xanthione and its methoxy derivatives absorption and fluorescence spectra

The calculations for several versions of the configuration interactions with different number of molecular orbitals were carried out: C.I. $= 4, 6, 8, 9$. Figure 3 shows the absorption and fluorescence spectra of the XT only for C.I. $= 9$ (the rest results are presented in supporting information in Figure S1). The absorption spectra obtained for C.I. $= 9$ are characterized by four well-defined lines corresponding to the main experimental bands. The energy diagram of XT is shown in Figure 4. The transitions between S_0 and S_2, S_4, S_9 states of XT molecule have considerably lower oscillator strengths comparing with the transition $S_{15} \leftarrow S_0$. Due to the symmetry of the molecule the oscillator strength of $S_1 \leftarrow S_0$ transition equals to zero. The fluorescence bands are calculated for optimized geometry of the S_2 and S_3 excited states.

The absorption and fluorescence spectra as well as energy diagram of two conformers of DXT are shown in Figures 5 and 6. The intensity of a transition to the first excited state does not equal to zero. That can be explained by broken symmetry of the compound due to the attachment of a methoxy group to a XT molecule. The transitions $S_3 \leftarrow S_0$ and $S_{15} \leftarrow S_0$ have oscillator strengths of the same order. For both conformers an additional line appears in the absorption spectra. Comparing the MECI calculations of the absorption band at 380–400 nm which is mainly due to $S_2 \leftarrow S_0$ and $S_3 \leftarrow S_0$ transitions for DXT with the experimental spectra we can conclude that in experimental spectrum both transition bands seem to have similar intensities. Therefore the mirror symmetry of absorption and fluorescence bands is broken. It should be noted that conformational changes influence slightly on the spectrum of the compound III. The latter can be explained by the fact that the conformational changes in the compounds III do not distort the XT skeleton in the ground electronic state. Comparing fluorescence spectra presented in Figures 3 and 5, one can see that the vibrational structure is smoothed in DXT although it is seen in the XT spectrum. Appearance of the additional line in the calculated absorption and fluorescence spectra can explain the reason of vibrational structure smoothing due to the overlap of two transitions.

In the case of XT there are minor shifts of the calculated lines relatively to that observed in experiments. For the compound III the simulated spectrum well reproduces a shift of the $S_2 \leftarrow S_0$ transition line to the blue in accordance with the experiment. The experimentally observed broadening of the band

ACCEPTED MANUSCRIPT

Table 3: The experimental and calculated (in parentheses) oscillator strengths of electronic transitions in XT and DXT. ε_{abs}^{max} is the extinction coefficient.

Compound	ε_{abs}^{max}, $M^{-1}cm^{-1}$	$S_1 \leftarrow S_0$	$S_2 \leftarrow S_0$	$S_3 \leftarrow S_0$	$S_4 \leftarrow S_0$	$S_{5(15)} \leftarrow S_0$
XT	10700	0 (0)	0.31 (4.52)	0.03 (1.13)	0.46 (5.27)	1.34 (26.41)
DXT	10000	$0(10^{-5})$	0.45 (0.44)	0.45 (5.51)	0.58 (2.25)	1.59 (11.02)

in the vicinity of 360 nm for the compound III relatively to the XT band can be associated with the appearance of additional transition $S_3 \leftarrow S_0$.

The luminescence spectra of XT and DXT shown in Figures 3 and 5 are consisted of two parts: fluorescence, $S_2 \rightarrow S_0$, being in the spectral region 400 – 600 nm and phosphorescence, $T_1 \rightarrow S_0$, (600–800 nm) [22]. The luminescence spectrum of DXT as well as its absorption spectrum reveals the hypsochromic shift relative to XT luminescence one. However, the shift $\Delta\nu_{fl} \simeq 300$ cm^{-1} evaluated as difference between $S_2 \rightarrow S_0$ fluorescence maxima of XT and DXT is 6 times smaller than $\Delta\nu_{abs} \simeq 1800$ cm^{-1} for $S_2 \leftarrow S_0$ absorption maxima. This fact can be explained by considerable variation of the normal vibrational frequencies of XT accompanying electronic excitation $S_2 \leftarrow S_0$. It is also interesting to note that there is a difference of full experimental widths at the half maximum of vibronic bands between XT ($\Delta\nu_{h/2} = 2950$ cm^{-1}) and DXT ($\Delta\nu_{h/2} = 4730$ cm^{-1}). At the same time the difference for the fluorescence bands (4200 cm^{-1} and 4800 cm^{-1}) is drastically smaller. The reason is the superposition of the two absorption bands $S_2 \leftarrow S_0$ and $S_3 \leftarrow S_0$. Increasing absorption band width in DXT is in agreement with quantum chemical calculations. The prediction of nonzero oscillator strength for $S_3 \leftarrow S_0$ transition that overlaps with $S_2 \leftarrow S_0$ transition explains the broadening of the band. At the same time fluorescence of DXT occurs from a single state that results in practically identical fluorescence band widths in XT and DXT. This is also supported by small hypsochromic shift of $S_2 \rightarrow S_0$ maximum from 448 nm to 442 nm and much larger shift (27 nm) for $S_2 \leftarrow S_0$. The parameters of stationary absorption and luminescence bands are listed in Table 4. Here the shifts $\Delta\nu_{band}$ are determined as the differences between corresponding experimental band maxima of DXT and XT, pictured in Figures 5 and 3.

The phosphorescence, $T_1 \rightarrow S_0$, in XT and DXT, also exhibits a hyp-

ACCEPTED MANUSCRIPT

Table 4: The characteristics of the stationary absorption and luminescence bands of the XT and DXT. The energy ($E_{\max}^{\text{band}}$) and the wavelength ($\lambda_{\max}$) of the corresponding band maximum. The shifts of the band maxima DXT relative to XT, $\Delta\nu_{\text{band}}$.

	XT		DXT		DXT vs XT
band	$E_{\max}^{\text{band}}$, eV	$\lambda_{\max}$, nm	$E_{\max}^{\text{band}}$, eV	$\lambda_{\max}$, nm	$\Delta\nu_{\text{band}}$, cm^{-1}
ph	1.851	670	1.968	630	950
abs1	1.962[a]	632	–[b]	–	–
fl2	2.755	450	2.805	442	406
abs2	3.100	400	3.221	385	975
abs3	4.039	307	4.052	306	105
abs4	4.863	255	4.769	260	−758
abs5	5.415	229	5.322	233	−750

[a] the value was taken from ref. 41
[b] the band was not observed

sochromic shift of the vibronic maximum from 670 nm in XT to 630 nm in DXT that amounts to $\Delta\nu_{\text{Ph}} \approx 950$ cm^{-1}. That shift is 2.4 times larger than $\Delta\nu_{\text{f}} \approx 400$ cm^{-1} for fluorescence maxima of XT and DXT.

Comparing the allowed $S_2 \rightarrow S_0$ and $T_1 \rightarrow S_0$ transitions of $\pi\,\pi^*$ type with the forbidden $S_1 \rightarrow S_0$ transition of $n\,\pi^*$ type, it can be assumed that attached methoxy groups weakly influence on $S_1 \rightarrow S_0$ transition. The quantum chemical calculations confirm the conclusion (see Figures 4 and 6). Consequently, the energy of S_1 state in DXT is close to that of XT. Since the locations of S_1 $n\,\pi^*$ and T_1 $\pi\,\pi^*$ states in XT[22] are 15970 cm^{-1} and 15130 cm^{-1}, respectively, the energies of these two states coincide with that in DXT. Therefore due to the intersystem crossing the total excitation energy of S_1 state deactivates through T_1 state.

The bands of absorption spectra for $S_1 \leftarrow S_0$ transition in Figures 3 and 5 are not shown since they are very weak. For example for XT the molar extinction coefficient 20 M^{-1}cm^{-1} and an oscillator strength of 0.0003 [42]. There is some difference between calculated and experimental results. The positions of the calculated absorption lines are shifted to the long-wave region, 740 nm, whereas in the experimental spectra such maxima $S_1 \leftarrow S_0$ are observed in the vicinity of 630 nm for XT [41].

To understand the nature of the spectra of the considered compounds,

ACCEPTED MANUSCRIPT

Table 5: The characteristics of the XT and DXT compounds in the electronic states: S_0, S_2, and S_3. Here q is a charge of corresponding atom. The dimensions of the quantities are the same as in Table 1. * The results presented in row 6 are obtained at the geometry termination optimization criteria: GNORM = 3. ** Results obtained at GNORM = 17.

No	Comp.	R_1	R_2	*State*	$\Delta_f H^\circ$	E_{tot}	μ	q_{C3}	q_{C7},	q_{C9}	q_S	$q_{O(R1)}$	$q_{O(R2)}$
1	I	H	H	S_0	34.18	-2141.762	3.875	-0.16	0.05	-0.16	-0.16	-	-
2	I	H	H	S_2	102.54	-2138.798	5.917	-0.1	-0.03	-0.1	-0.31	-	-
3	I	H	H	S_3	113.25	-2138.334	6.198	-0.11	-0.19	-0.11	-0.28	-	-
4	III	H_3CO(cis)	H_3CO	S_0	-33.13	-3027.143	4.251	-0.22	0.07	-0.16	-0.17	-0.19	-0.15
5	III	H_3CO(cis)	H_3CO	S_2	34.48	-3024.211	5.451	-0.12	-0.02	-0.12	-0.29	-0.17	-0.12
6*	III	H_3CO(cis)	H_3CO	S_3	41.75	-3023.895	6.233	-0.14	-0.16	-0.08	-0.25	-0.19	-0.08
7	III	H_3CO(trans)	H_3CO	S_0	-33.15	3027.144	4.925	-0.22	0.07	-0.16	-0.17	-0.19	-0.15
8	III	H_3CO(trans)	H_3CO	S_2	42.13	-3023.879	6.888	-0.15	-0.11	-0.12	-0.25	-0.2	-0.05
9**	III	H_3CO(trans)	H_3CO	S_3	41.98	-3023.886	7.269	-0.14	-0.17	-0.09	-0.26	-0.2	-0.05

calculations of energies of the excited states S_2 and S_3 were performed with full geometry optimization. The results are listed in Table 5. According to the calculations, the excitation of S_2 state results in considerable variation of the sulfur charge and increase of the bond length between C_7 and the sulfur by 0.2 Å. The charges on C_3 and C_9 also slightly vary. Since the area where a variation of the atomic charges is not bulky the alteration of the dipole moment is not strong. In XT derivatives containing a methoxy group the oxygen charge may noticeably vary but only for some their conformers. Thus, methoxy group demonstrates its electron-donor origin.

3.3. Transient spectra of XT and DXT

The transient time-resolved spectra of XT and DXT do not have great differences. Our femtosecond measurements of XT and DXT in n-hexane at room temperature allowed to reveal the transient absorption spectra at $\lambda_{max} \simeq 650$ nm and gain spectra at $\lambda_{max} \simeq 480$ nm. The kinetics of TA signal at 475 nm consist of two components: the short component with a lifetime about 20 ps and very long-lived one exceeding 100 ps. Apparently, the first short lifetime of 20 ps associates with the excited S_2 state decay and long time constant probably characterizes rising the triplet triplet $T_k \leftarrow T_1$ absorption.

The femtosecond measurements of XT and DXT in n-hexan at room temperature in the wavelength domain from $\lambda = 400$ to 740 nm in the time window from 1 ps to 100 ps were carried out. The transient time-resolved spectra of XT and DXT are presented in Figures 7.

ACCEPTED MANUSCRIPT

The complex dynamics of experimental transient spectra shown in Fig. 7 leads to the supposition that there are several constituents. Among them the most pronounced are: two excited-state absorption bands, $S_2 \to S_n$ and $S_1 \to S_m$, stimulated emission, $S_2 \to S_0$, triplet-triplet absorption, $T_1 \to T_k$ and the bleach (the bleach is not shown because it was out of the experimental spectral window). The transient spectra of DXT pictured in Fig. 7 are similar to XT spectra but there are differences. DXT spectra consist at least of six constituents: two excited-state absorption bands, $S_2 \to S_n$, the excited state absorption $S_1 \to S_m$, stimulated emission, $S_2 \to S_0$ and triplet-triplet absorption, $T_1 \to T_k$ and the bleach.

For quantitative description of spectral evolution the theory reported in ref [43] has been adopted. The transitions $S_2 \to S_1 \to T_1$ are considered to be exponential. The simulations confirm the adopted schema of electronic transitions in excited XT and DXT: the initially excited S_2 states decay due to internal conversion to S_1 state with time constant τ_{IC} that subsequently decays due to intersystem crossing to populate the triplet state T_1 with time constant τ_{ISC}.

The transient absorption signal ΔA in the pump-probe technique can be represented as follows [43]

$$\Delta A(\omega_e, \omega_p, \tau) = \sum_i \Delta A_i(\omega_e, \omega_p, \tau) P_j(\tau) \tag{1}$$

where the subscript i runs through the values $i = \{\mathrm{ESA}k, \mathrm{TTA}, \mathrm{SE}, \mathrm{BL}\}$ accounting for the k-th excited-state absorption, $\Delta A_{\mathrm{ESA}k}$, the triplet-triplet absorption, ΔA_{TTA}, stimulated emission, ΔA_{SE}, and bleach, ΔA_{BL}, the index j can take any value from the following list of the electronic states $\{S_2, S_1, T_1, S_0\}$:

$$\Delta A_i(\omega_e, \omega_p, \tau) = \omega_p w_i \frac{V_p^2}{P} \frac{\pi \tau_p}{\sigma_i(\tau)} \sum_{n,m} P_n \frac{e^{-\xi_i} \xi_i^m}{m!} \times$$

$$\times \exp\left[-\frac{(\delta\omega_{mi} - Q_{ni}(\tau))^2}{2\sigma_i^2(\tau)} \right]. \tag{2}$$

Here w_i is the weight of corresponding band, $\sigma_i(\tau)$ and $Q_{ni}(\tau)$ are the values of the time-dependent half-width and the coordinate of the center-of-gravity of the corresponding band:

$$\sigma_i^2(\tau) = \tau_p^{-2} + 2E_{ri}k_BT - (2E_{ri}k_BTX(\tau)/\sigma_e^2)^2, \tag{3}$$

ACCEPTED MANUSCRIPT

$$Q_{ni}(\tau) = 2E_{ri}X(\tau)(1 - \delta_{i,BL} + \delta\omega_{ne}k_BT/\sigma_e^2), \tag{4}$$

where E_{ri} is the reorganization energy of the solvent for i-th transition, $\xi_i = E_{rhi}/\Omega_{hf}$ is the Huang-Rhys factor, E_{rhi} and Ω_{hf} are the reorganization energy and frequency of the high-frequency mode for a corresponding transition. The rest of parameters is $\delta\omega_{ne} = \omega_e + \Delta G_{SE} - E_{rSE} - n\Omega_{hf}$, $\delta\omega_{mESAk} = \omega_p + \Delta G_{ESAk} - E_{rESAk} - m\Omega_{hf}$, $\delta\omega_{mTTA} = \omega_p + \Delta G_{TTA} - E_{rTTA} - m\Omega_{hf}$, $\delta\omega_{mSE} = \omega_p + \Delta G_{SE} + E_{rSE} + m\Omega_{hf}$, $\delta\omega_{mBL} = \omega_p + \Delta G_{SE} - E_{rSE} - m\Omega_{hf}$, where ΔG_i are the free energies for ESAk, TTA, SE, and BL. $P = \sum P_n$, where P_n is the probability of the transition generating n vibrational quanta during the pump stage:

$$P_n = \frac{\pi V_e^2 \tau_e}{\sigma_e} \frac{e^{-\xi_{SE}} \xi_{SE}^n}{n!} \exp\left[-\frac{(\delta\omega_{ne})^2}{2\sigma_e^2}\right], \tag{5}$$

$\sigma_e^2 = \tau_e^{-2} + 2E_{rSE}k_BT$. Here τ_p and ω_p are the duration and frequency of the probe pulse, τ_e and ω_e are the duration and carrier frequency of the pump pulse, $\delta_{\mathbf{i,BL}}$ is the Kronecker delta, k_B and T – the Boltzmann constant and the temperature, respectively, the Planck constant is set to be equal to unity, $\hbar = 1$. V_e and $\mathbf{V_p}$ are the matrix elements of the dipole interaction with the electromagnetic wave field strength for the pump and probe pulses. The spectral dynamics is supposed to be much slower than the intramolecular vibrational redistribution and relaxation. This is the reason why the vibrational relaxation is considered to be instant. $X(t) = \sum_{i=1}^{2} x_i e^{-t/\tau_i}$ is the relaxation function of the solvent. The populations kinetics of the excited states S_2, S_1, and T_1 are

$$P_{S2}(t) = e^{-t/\tau_{IC}}\,, \tag{6}$$

$$P_{S1}(t) = \frac{(e^{-t/\tau_{IC}} - e^{-t/\tau_{ISC}})\tau_{IC}}{\tau_{IC} - \tau_{ISC}}\,, \tag{7}$$

$$P_{T1}(t) = 1 - \frac{e^{-t/\tau_{IC}}\tau_{IC} - e^{-t/\tau_{ISC}}\tau_{ISC}}{\tau_{IC} - \tau_{ISC}}\,, \tag{8}$$

where τ_{IC} and τ_{ISC} are the internal conversion and the intersystem crossing time constants, respectively. The nonradiative channel $S_2 \leftarrow S_0$ is too weak to be include in consideration. The model does not take into account the ground state recovery because the main channel of decay of S_2 is $S_2 \rightarrow S_1 \rightarrow T_1$ and the lifetime of T_1 is much larger than the timescale of the transient

ACCEPTED MANUSCRIPT

absorption experiment. That is the reason why the ground state does not recovery, hence, its population is constant, $P_{S0} = 1$.

The parameters fixed for all calculations are following: $k_BT = 0.25$ eV, $\Omega_{hf} = 0.15$ eV, $\omega_e = 3.1$ eV, $\tau_e = \tau_p = 100$ fs, $V_p = 0.005$ eV. The parameters are set to satisfy the experimental setup. The vibrational frequency is determined from the structure of the XT fluorescence band. The dynamics of the experimental transient spectra is not very fast and the solvent relaxation does not manifest itself. This means that the time scale of the solvent relaxation is much shorter than that of electronic transitions. Since the dielectric solvation in nonpolar solvents is insignificant, the response of a solvent on the alteration of volume of a molecule accompanying electronic transition is an important part of the reorganization of such solvents. The relaxation of such a response should correlate with its viscosity [44]. The dynamics parameters of n-hexane are not known. Since n-hexane has rather low viscosity its relaxation is expected to be fast: $\tau_1 = 100$ fs, $\tau_2 = 600$ fs, $x_1 = 0.6$, $x_2 = 0.4$. The parameters obtained in the fitting are listed in Tables 6 and 7. A similar approach to transient absorption spectra modelling was used in recent publication [45].

Table 6: The model parameters are fitted from TA spectra of XT. E_{max} is the energy of the maximum of the corresponding band. All the energies are in eV.

No	i	w_i	j	E_{ri}	E_{rhi}	ΔG_i	E_{max}
1	ESA2	1.4	S2	0.1	0.12	-1.82	2.04
2	ESA1	1.4	S1	0.1	0.12	-1.88	2.10
3	SE	0.8	S2	0.1	0.37	-2.97	2.50
4	TTA	0.8	T1	0.1	0.16	-2.57	2.83
5	BL	0.2	S0	0.1	0.37	-2.97	3.44

Table 7: The model parameters are fitted from TA spectra of DXT. E_{max} is the energy of the maximum of the corresponding band. All the energies are in eV.

No	i	w_i	j	E_{ri}	E_{rhi}	ΔG_i	E_{max}
1	ESA3	0.6	S2	0.12	0.18	-1.70	2.00
2	ESA2	1.15	S2	0.12	0.12	-2.72	2.96
3	ESA1	1.15	S1	0.12	0.12	-2.72	2.96
4	SE	0.5	S2	0.12	0.38	-2.92	2.34
5	TTA	0.3	T1	0.12	0.14	-2.46	2.72
6	BL	0.5	S0	0.12	0.37	-2.97	3.46

For both XT and DXT the negative signal in the area around 480 nm

ACCEPTED MANUSCRIPT

predominantly consists of the stimulate emission $S_2 \rightarrow S_0$ but there is a considerable overlapping with ESAk and TTA bands. Triplet-triplet absorption leads to a positive signal in the area of 450 nm when time exceeds 10 and 40 ps in XT and DXT, correspondingly. For XT the wavelength of triplet-triplet absorption is in good agreement with data from reference [32]. Overlapping of the bands requires modelling of transient spectra for determining the time constants of the internal conversion $S_2 \rightarrow S_1$ and intersystem crossing $S_1 \rightarrow T_1$. Analysis of decay kinetics of the signal at 499 gives $\tau_{IC} = 20.0$ and at 523 nm gives $\tau_{IC} = 28.0$ ps. The fitting by using Eq. 1 allows determination of both the internal conversion and intersystem crossing time constants. They are $\tau_{IC} = 14.0$ and $\tau_{ISC} = 17.0$ ps for XT and $\tau_{IC} = 26.0$ and $\tau_{ISC} = 20.0$ ps for DXT. Larger difference in estimations of τ_{IC} for XT is caused by larger overlapping of the stimulated emission $S_2 \rightarrow S_0$ and excited state absorption bands from the S_1 and S_2 states in the red wing.

To fit the transient spectra of XT and DXT a few ESA bands are exploited. The energies of ESAk maxima obtained from the fitting are listed in Tables 6 and 7. Their values well correlate with data obtained from stationary absorption spectra. For example, ESA from the second excited state has a maximum at 2.04 eV that is close to the difference of the energies $E^{abs4}_{max} - E^{fl2}_{max} = 4.86 - 2.75 = 2.11$ eV (see Table 4). ESA from the first excited state has a maximum at 2.10 eV that is close to the difference of the energies $E^{abs3}_{max} - E^{ph}_{max} = 4.04 - 1.85 = 2.19$ eV. Similar correlations can be obtained for DXT if one supposes that the S_1 energy level is higher than the T_1 level by a few $k_{\mathrm{B}}T$.

The kinetic curves for several selected wavelengths are shown in Figures 8 and 9 for XT and DXT. The figures also demonstrate the contributions of the constituents to the total signal depicted by colored curves. The necessity of accounting for $S_1 \rightarrow S_n$ absorption in XT is well seen from the signal kinetics at 599 and 635 nm pictured in Figure 8. $S_2 \rightarrow S_n$ absorption in DXT is also seen at 419 and 433 nm in Figure 9.

Despite the simplicity of the kinetic model Eqs. 6 – 8 applied to each separate constituent, the total signal at selected wavelengths is well reproduced in whole. The negligible deviations of the simulated curves from experimental data are apparently caused by weak excited state absorption bands that are not included in the model.

ACCEPTED MANUSCRIPT

4. CONCLUSIONS

The quantum chemical calculations of methoxy derivatives of the XT molecule in the ground electronic state reveal an influence of methoxy groups on the XT geometry and electronic structure. It is ascertained that only the compound III demonstrates remarkable geometry changes. Therefore the deformation of the XT skeleton plane may result in the appearance of enantiomer properties.

A comparison of MECI calculations of the pure XT and its methoxy derivative shows a shift and pronounced broadening of absorption spectra band of newly synthesized compound III relatively to the band of the compound I. The experimentally observed broadening for the compound III can apparently be associated with the manifestation of transition $S_3 \leftarrow S_0$ that is forbidden in XT. The calculations of the second excited state of XT and its methoxy derivative confirm noticeable charge transfer (about 0.1 of the charge of an electron) from the methoxy group to the thiocarbonyl group.

The fitting of the transient spectra measured in n-hexane has shown that the decay time constants of XT and DXT S_2 state population considerably differ amounting 14.0 and 26.0 ps, respectively. That presumably evidences that the charge transfer in DXT is not sufficiently large to effectively quench the second excited electronic state by electron transfer. The primary channel of the second excited state deactivation is the internal conversion in the both XT and DXT with subsequent intersystem crossing to T_1. The time constants of the intersystem crossing $S_1 \rightarrow T_1$ for XT and DXT amount to 17.0 and 20 ps, correspondingly and is comparable with the lifetime of S_2 state.

Noticeable enlarging the S_2 state lifetime in DXT relatively to XT is probably caused by the increase of the energy gap between the first and second excited states and partial charge transfer from the methoxy to thiocarbonyl groups. Thus, methoxi derivatives of XT may be perspective molecules for molecular devices exploiting the second excited state.

ACKNOWLEDGMENTS

This work was supported by the Russian Foundation for Basic Research (Grants No. 16-53-00189) and the Belarusian Republican Foundation for Fundamental Research (Grants No. C16R-104).

ACCEPTED MANUSCRIPT

[1] E. Greenbaum, Biomolecular electronics and applications, in: R. Meyers (Ed.), Molecular biology and biotechnology: A comprehensive desk reference, Wiley-VCH, Inc., Toronto, 1995, pp. 98–106.

[2] S.-S. Sun, L. R. Dalton (Eds.), Introduction to organic electronic and optoelectronic, Taylor & Francis Group, LLC, Boca Raton, FL, 2008, p. 936.

[3] O. Ostroverkhova, Organic optoelectronic materials: mechanisms and applications, Chem. Rev. 116 (2016) 13279–13412. doi:10.1021/acs.chemrev.6b00127.

[4] M. Sauer, P. Tinnefeld, Molecular optical switches and waveguides. new concepts of tiny electronic devices, Optic & Photonik 2 (2007) 45–48. doi:10.1002/opph.201190251.

[5] S. Wallin, C. Monnereau, E. Blart, J.-R. Gankou, F. Odobel, L. Hammarström, State-selective electron transfer in an unsymmetric acceptor-Zn(II)porphyrin-acceptor triad: toward a controlled directionality of electron transfer from porphyrin S_2 and S_1 states as a basis from molecular switch, J. Phys. Chem. A 114 (2010) 1709–1721. doi:10.1021/jp907824d.

[6] M. Andersson, J. Davidsson, L. Hammarström, J. Korppi-Tommola, T. Peltola, Photoinduced electron transfer reactions in a porphyrin- viologen complex: observation of S_2 to S_1 relaxation and electron transfer from S_2 state, J. Phys. Chem. B 103 (1999) 3258–3262. doi:10.1021/jp9829795.

[7] N. Mataga, Y. Shibata, H. Chosrowjan, N. Yoshida, A. Osuka, Internal conversion and vibronic relaxation from higher excited state of porphyrins: femtosecond fluorescence dynamics studies, J. Phys. Chem. B 104 (2000) 4001–4004. doi:10.1021/jp9941256.

[8] P.-A. Muller, E. Vauthey, Charge recombination dynamics of geminate ion pairs formed by electron transfer quenching of molecules in an upper excited state, J. Phys. Chem. A 105 (2001) 5994–6000. doi:0.1021/jp010015z.

ACCEPTED MANUSCRIPT

[9] A. Morandeira, L. Engeli, E. Vauthey, Ultrafast charge recombination of photogenerated ion pairs to an electronic excited state, J. Phys. Chem. A 106 (2002) 4833–4837. doi:10.1021/jp014393f.

[10] N. Mataga, S. Tanigushi, H. Chosrowjan, A. Osuka, N. Yoshida, Ultrafast charge transfer and radiationless relaxations from higher excited state (S_2) of directly linked zinc-porphyrin (ZP)-acceptor dyads: investigations into fundamental problems of exciplex chemistry, Chem. Phys. 295 (2003) 215–228. doi:10.1016/j.chemphys.2003.09.005.

[11] M. Kubo, Y. Mori, M. Otani, M. Murakami, Y. Ishibashi, M. Yasuda, K. Hosomuzu, H. Imahori, S. Nakashima, Ultrafast photoinduced electron transfer in directly linked porphyrin-ferrocene dyads, J. Phys. Chem. A 111 (2007) 5136–5143. doi:10.1021/jp071546b.

[12] M. Fujitsuka, D. W. Cho, S. Tojo, A. Inoue, T. Shiragami, M. Yasuda, T. Majima, Electron transfer from axial ligand to S_1- and S_2-excited phosphorus tetraphenylporphyrin, J. Phys. Chem. A 111 (2007) 10574–10579. doi:10.1021/jp076303y.

[13] V. N. Ionkin, A. I. Ivanov, Numerical simulations of ultrafast charge separation dynamics from second excited state of directly linked zinc-porphyrin-imide dyads and ensuring hot charge recombination into the first excited state, J. Phys. Chem. A 113 (2009) 103–107. doi:10.1021/jp806589m.

[14] M. V. Rogozina, V. N. Ionkin, A. I. Ivanov, What factors control product yield in charge separation reaction from second excited state in zinc-porphyrin derivatives?, J. Phys. Chem. A 116 (4) (2012) 1159–1167. doi:10.1021/jp210988k.

[15] M. V. Rogozina, V. N. Ionkin, A. I. Ivanov, Dynamics of charge separation from second excited state and following charge recombination in zinc-porphyrin-acceptor dyads, J. Phys. Chem. A 117 (2013) 4564–4573. doi:10.1021/jp402734h.

[16] B. Robotham, K. A. Lastman, S. J. Langford, K. P. Ghiggino, Ultrafast electron transfer in a porphyrin-amino naphthalene diimide dyad, J. Photochem. Photobiol. A 251 (2013) 167–174. doi:10.1016/j.jphotochem.2012.11.002.

ACCEPTED MANUSCRIPT

[17] S. V. Feskov, A. I. Ivanov, Efficiency of intramolecular charge separation from the second excited state: suppression of the hot charge recombination by electron transfer to the secondary acceptor, J. Phys. Chem. A 117 (45) (2013) 11479–11489. doi:10.1021/jp408516q.

[18] M. V. Rogozina, V. N. Ionkin, A. I. Ivanov, Kinetics of charge separated state population produced by intramolecular electron transfer quenching of second excited state, J. Photochem. Photobiol. A 301 (2015) 55–61. doi:10.1016/j.jphotochem.2015.01.002.

[19] S. V. Feskov, A. I. Ivanov, Effect of geometrical parameters of dyad $d-a$ and triad $d-a_1-a_2$ on the efficiency of ultrafast intramolecular charge separation from second excited state, Chem. Phys. 478 (2016) 164–172. doi:10.1016/j.chemphys.2016.03.013.

[20] S. V. Feskov, V. A. Mikhailova, A. I. Ivanov, Non-equilibrium effects in ultafast photoinduced charge transfer kinetics, J. Photochem. Photobiol. C 29 (2016) 48–72. doi:10.1016/j.jphotochemrev.2016.11.001.

[21] V. Ramamurthy, K. S. Shanze (Eds.), Organic photochemistry and photophysics, Vol. 14, Taylor & Francis Group, LLC, Boca Raton, FL, 2006, p. 300.

[22] A. Maciejewski, R. P. Steer, The photophysics, physical photochemistry, and related spectroscopy of thiocarbonyls, Chem. Rev. 93 (1993) 67–98. doi:10.1021/cr00017a005.

[23] N. O. Obi-Egbedi, I. B. Obot, M. I. El-Khaiary, Quantum chemical investigation and statistical analysis of the relationship between corrosion inhibition efficiency and molecular structure of xanthene and its derivatives on mild steel in sulphuric acid, J. Mol. Struct. 1002 (1–3) (2011) 86–96. doi:10.1016/j.molstruc.2011.07.003.

[24] A. Maciejewski, R. P. Steer, Photophysics of the second excited singlet states of xanthione and related thiones in perfluoroalkane solvents, J. Am. Chem. Soc. 105 (1983) 6738–6740. doi:10.1021/ja00360a046.

[25] J. J. P. Stewart, Optimization of parameters for semiempirical methods I. method., J. Comput. Chem. 10 (1989) 209–220. doi:10.1002/jcc.540100208.

ACCEPTED MANUSCRIPT

[26] J. J. P. Stewart, Comparison of the accuracy of semiempirical and some dft methods for predicting heats of formation, J. Mol. Model 10 (2004) 6–12. doi:10.1007/s00894-003-0157-6.

[27] J. J. P. Stewart, Use of semiempirical methods for detecting anomalies in reported enthalpies of formation of organic compounds, J. Phys. Chem. Ref. Data 33 (2004) 713–724. doi:10.1063/1.1643403.

[28] G. B. Rocha, R. O. Freire, A. M. Simas, J. J. P. Stewart, RM1: A reparameterization of AM1 for H, C, N, O, P, S, F, Cl, Br, and I, J. Comput. Chem. 27 (2006) 1101–1111. doi:10.1002/jcc.20425.

[29] J. J. P. Stewart, Optimization of parameters for semiempirical methods II. applications., J. Comput. Chem. 10 (1989) 221–264. doi:10.1002/jcc.540100209.

[30] A. Klamt, G. Scüümann, COSMO. a new approach to dielectric screening solvents with explicit expressions for the screening energy and its gradient, J. Chem. Soc., Perkin Trans. 2 (5) (1993) 799–805. doi:10.1039/P29930000799.

[31] D. R. Armstrong, R. Fortune, P. G. Perkins, Molecular orbital theory for the excited state of transition metal complexes, J. Chem. Soc., Faraday Trans. 2 68 (1972) 1839–1846. doi:10.1039/F29726801839.

[32] M. Szymanski, M. Balicki, M. Binkowski, J. Kubicki, A. Maciewski, E. Pawlowska, T. Wrozowa, Effects of solute-solvent interactions on radiationless decay of thioketones excited to their s-2-states and t-1-states, Acta Physica Polonica A 89 (1996) 527–544. doi:10.12693/APhysPolA.89.527.

[33] N. G. Bakhshiev, M. I. Knyazhanskii, V. I. Minkin, O. A. Osipov, G. V. Saidov, Experimental determination of the dipole moments of organic molecules in excited electronic states, Russ. Chem. Rev. 38 (9) (1969) 740–754. doi:10.1070/RC1969v038n09ABEH001831.

[34] N. A. Borisevich, O. V. Bouganov, S. A. Tikhomirov, G. B. Tolstorozhev, G. L. Shkred, Passive mode locking of a femtosecond ti:sapphire laser with pulsed synchronous pumping by a finite train of picosecond pulses, Quant. Electron. 29 (1999) 780–786. doi:10.1070/QE1999v029n09ABEH001572.

ACCEPTED MANUSCRIPT

[35] V. I. Stsiapura, S. A. Kurhuzenkau, V. A. Kuzmitsky, O. V. Bouganov, S. A. Tikhomirov, Solvent polarity effect on nonradiative decay rate of thioflavin T, J. Phys. Chem. A 120 (28) (2016) 5481–5496. doi:10.1021/acs.jpca.6b02577.

[36] H. Y. Afeefy, J. F. Liebman, S. E. Stein, Neutral thermochemical data, in: P. J. Linstrom, W. G. Mallard (Eds.), NIST Chemistry WebBook. NIST Standard Reference Database Number 69, National Institute of Standards and Technology, Gaithersburg, MD, 20899, (retrieved March 10, 2017).
URL http://webbook.nist.gov

[37] M. V. Roux, M. Tompardo, J. C. Chickos, Y. Nagano, Critacally evaluated thermodynamical properties of polycyclic aromatic hydrocarbons, J. Phys. Chem. Ref. Data 37 (2008) 1855–1996. doi:10.1063/1.2955570.

[38] J. O. Fenwick, D. Harrop, A. J. Head, Thermodynamic properties of organic oxigen compounds 41. enthalpies of formation of eight ethers, J. Chem. Thermodyn. 7 (1975) 943–954. doi:10.1016/0021-9614(75)90158-5.

[39] J. D. Cox, G. Plicher, Thermochemistry of organic and organomethallic compounds, Academic Press, New York, 1970.

[40] R. Sabbah, L. E. Watik, Etude therodynamique de l'acridone et de la thioxanthone, Can. J. Chem. 70 (1992) 24–28. doi:10.1139/v92-005.

[41] J. R. Huber, M. Mahaney, $S_2 \rightarrow S_0$ fluorescence in an aromatic thiokethone, xanthione, Chem. Phys. Lett. 30 (1975) 410–412. doi:10.1016/0009-2614(75)80019-4.

[42] D. A. Capitanio, H. J. Pownall, J. R. Huber, Spectroscopic and photochemical properties of aromatic thioketones: xanthione, J. Photochem. 3 (1) (1974) 225–236. doi:10.1016/0047-2670(74)80022-5.

[43] R. G. Fedunov, A. I. Ivanov, Influence of spectral characteristics of the pump pulse on the transient absorption of donoracceptor complexes in polar solvents, J. Russ. Laser Res. 33 (2) (2012) 152–165. doi:10.1007/s10946-012-9269-8.

ACCEPTED MANUSCRIPT

[44] A. I. Ivanov, Hydrodynamic model of complex volume fluctuations interactions with medium and its influence on the rate of outer-sphere electron transfer, Russian J. Chem. Phys. 9 (1990) 1276–1282.

[45] R. G. Fedunov, A. Plotnikova, A. I. Ivanov, E. Vauthey, Simulations of the ultrafast transient absorption dynamics of a donor-acceptor biaryl in solution, J. Phys. Chem. A 121 (2) (2017) 471–481. doi:10.1021/acs.jpca.6b11581.

ACCEPTED MANUSCRIPT

ACCEPTED MANUSCRIPT

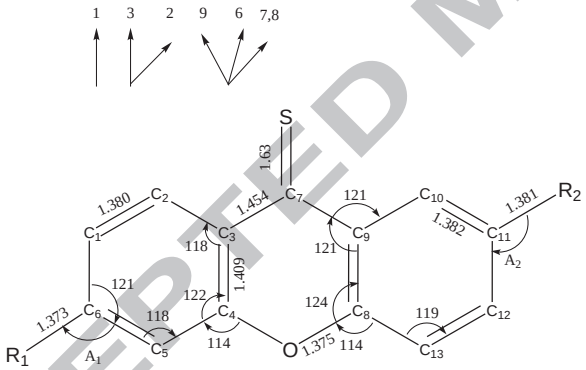

Figure 1: The geometry structure of XT derivatives in the ground state for compounds: I, II, and IV. The arrows show the dipole moment directions for a number of conformers. The conformer numeration is given in Table 1.

ACCEPTED MANUSCRIPT

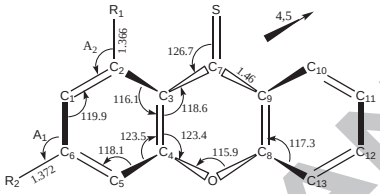

Figure 2: The geometry structure of XT derivatives in the ground state for compound III. The arrows show the dipole moment directions.

ACCEPTED MANUSCRIPT

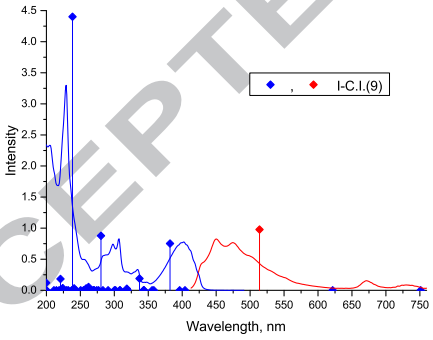

Figure 3: The absorption and luminescence spectra of XT in n-hexane solvent. The solid lines correspond to experimental results for absorption (blue) and luminescence (red). The vertical lines show the results of calculation. The numbers of C.I. are listed in Figure.

ACCEPTED MANUSCRIPT

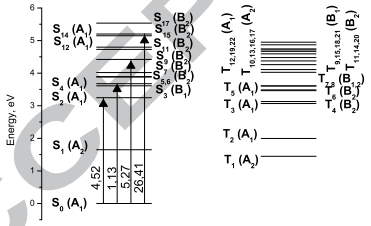

Figure 4: The energy level diagram of XT for C.I. = 9. The arrows show only the transitions with considerable oscillator strength. The numbers correspond to the values of the non-normalized oscillator strength as MOPAC 2016 produces.

ACCEPTED MANUSCRIPT

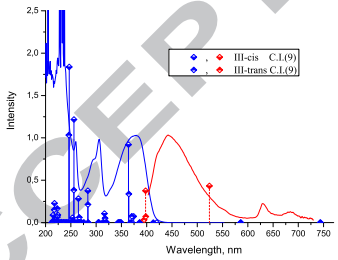

Figure 5: The absorption and luminescence spectra of DXT in n-hexane solvent. The solid lines correspond to experimental results for absorption (blue) and luminescence (red). The vertical lines show the results of calculation for C.I. = 9.

ACCEPTED MANUSCRIPT

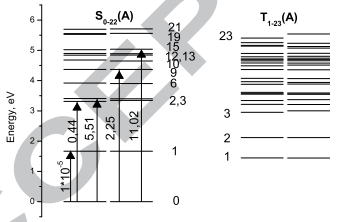

Figure 6: The energy level diagram of the DXT for C.I. = 9. The left and right columns correspond to the cis- and trans-conformers. The arrows show only the transitions with considerable oscillator strength. The numbers correspond to the values of the non-normalized oscillator strength as MOPAC 2016 produces.

ACCEPTED MANUSCRIPT

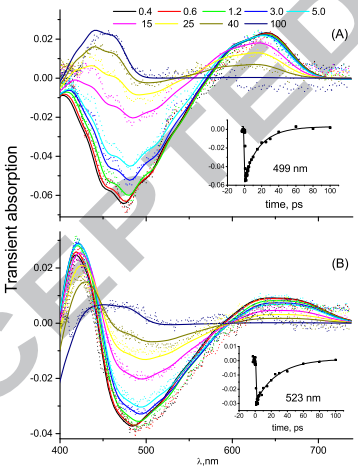

Figure 7: The experimental (dotted lines) and simulated (solid lines) transient absorption spectra of XT (Frame A) and DXT (Frame B) in n-hexane. The theoretical curves were calculated by using model given by Eq. 6–8. In the inserts the kinetic curve at 499 nm (A) and 523 nm (B) are shown with dots and their biexponential fitting are pictured. The energetic parameters obtained in the fitting are listed in the text.

ACCEPTED MANUSCRIPT

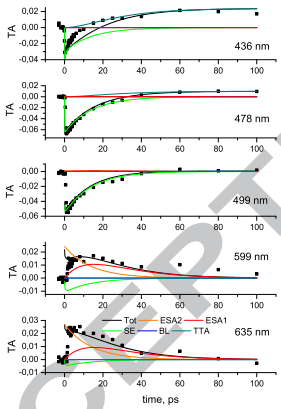

Figure 8: The experimental (dotted lines) and simulated (solid lines) kinetic curves at several wavelengths for XT in n-hexane. The constituents of the total signal are shown colored lines. The calculation parameters obtained from the fitting are listed in the text.

ACCEPTED MANUSCRIPT

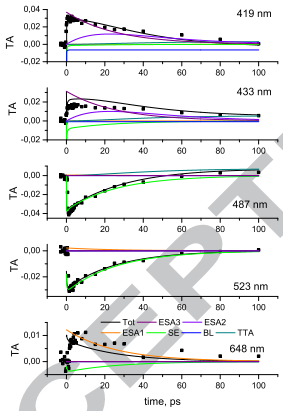

Figure 9: The experimental (dotted lines) and simulated (solid lines) kinetic curves at several wavelengths for DXT in n-hexane. The constituents of the total signal are shown colored lines. The calculation parameters obtained from the fitting are listed in the text.

ACCEPTED MANUSCRIPT

1,3-dimethoxy-9H-xanthene-9-thione

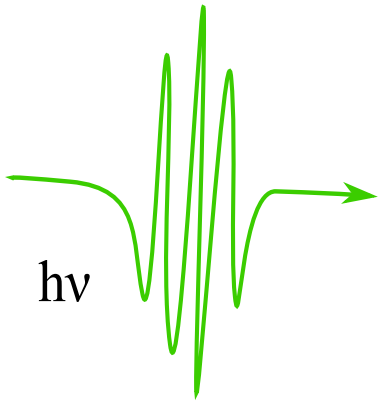

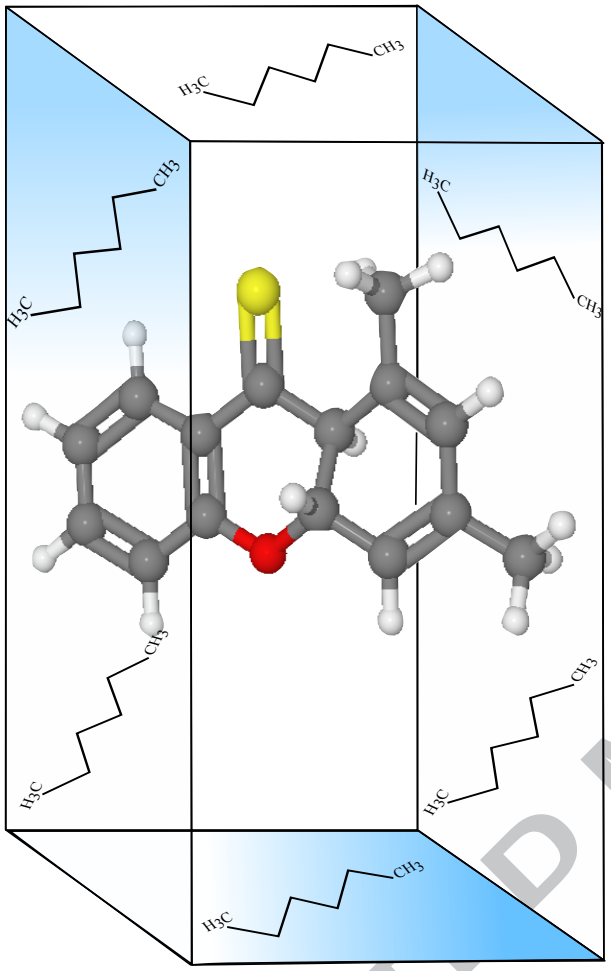

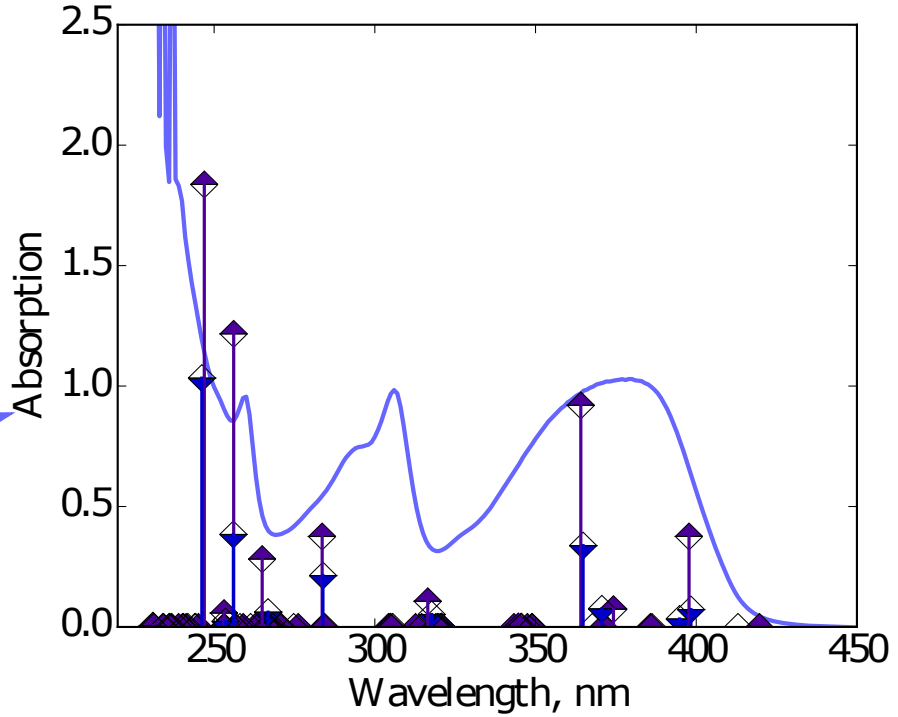

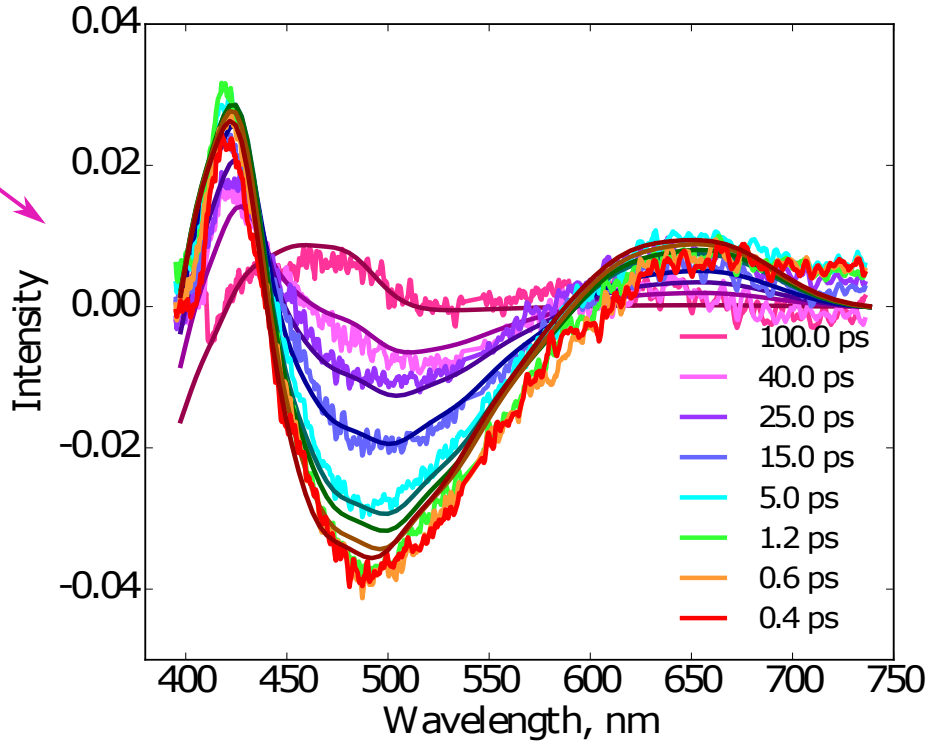

ACCEPTED MANUSCRIPT

Highlights

- A methoxy derivative of xantione was synthesized its stationary and transient spectra were measured.
- Time constants of internal conversion $S_2 \rightarrow S_1$ and intersystem crossing $S_1 \rightarrow T_1$ are determined for xantione and its methoxy derivative.
- Attachment of methoxy groups to xantione increases the S_2 state lifetime.

ACCEPTED MANUSCRIPT